

Suppression of stimulated Brillouin and Raman scatterings using an alternating frequency laser and transverse magnetic fields

Rui-Jin Cheng(程瑞锦), Xiao-Xun Li(李晓旬), Qing Wang(王清), De-Ji Liu(刘德基), Zhuo-Ming Huang(黄卓明), Shuai-Yu Lv(吕帅宇), Yuan-Zhi Zhou(周远志), Shu-Tong Zhang(张舒童), Xue-Ming Li(李雪铭), Zu-Jie Chen(陈祖杰), Qiang Wang(王强), Zhan-Jun Liu(刘占军), Li-Hua Cao(曹莉华), and Chun-Yang Zheng(郑春阳)
Citation: Chin. Phys. B, 2024, 33 (**1**): 015206. DOI: 10.1088/1674-1056/ad0716
Journal homepage: http://cpb.iphy.ac.cn; http://iopscience.iop.org/cpb

What follows is a list of articles you may be interested in

Nonlinear mixing-based terahertz emission in inclined rippled density plasmas

K Gopal, A P Singh, and S Divya
Chin. Phys. B, 2023, 32 (**6**): 065202. DOI: 10.1088/1674-1056/aca9c9

Intense low-noise terahertz generation by relativistic laser irradiating near-critical-density plasma

Shijie Zhang(张世杰), Weimin Zhou(周维民), Yan Yin(银燕), Debin Zou(邹德滨), Na Zhao(赵娜), Duan Xie(谢端), and Hongbin Zhuo(卓红斌)
Chin. Phys. B, 2023, 32 (**3**): 035201. DOI: 10.1088/1674-1056/ac872c

Correction of intense laser-plasma interactions by QED vacuum polarization in collision of laser beams

Wen-Bo Chen(陈文博) and Zhi-Gang Bu(步志刚)
Chin. Phys. B, 2023, 32 (**2**): 025204. DOI: 10.1088/1674-1056/ac70b3

Effects of Landau damping and collision on stimulated Raman scattering with various phase-space distributions

Shanxiu Xie(谢善秀), Yong Chen(陈勇), Junchen Ye(叶俊辰), Yugu Chen(陈雨谷), Na Peng(彭娜), and Chengzhuo Xiao(肖成卓)
Chin. Phys. B, 2022, 31 (**5**): 055201. DOI: 10.1088/1674-1056/ac3ba7

Influence of a centered dielectric tube on inductively coupled plasma source: Chamber structures and plasma characteristics

Zhen-Hua Bi(毕振华), Yi Hong(洪义), Guang-Jiu Lei(雷光玖), Shuai Wang(王帅), You-Nian Wang(王友年), Dong-Ping Liu(刘东平)
Chin. Phys. B, 2017, 26 (**7**): 075203. DOI: 10.1088/1674-1056/26/7/075203

Suppression of stimulated Brillouin and Raman scatterings using an alternating frequency laser and transverse magnetic fields

Rui-Jin Cheng(程瑞锦)[1], Xiao-Xun Li(李晓旬)[1], Qing Wang(王清)[1], De-Ji Liu(刘德基)[1], Zhuo-Ming Huang(黄卓明)[1], Shuai-Yu Lv(吕帅宇)[1], Yuan-Zhi Zhou(周远志)[2], Shu-Tong Zhang(张舒童)[2], Xue-Ming Li(李雪铭)[1], Zu-Jie Chen(陈祖杰)[2], Qiang Wang(王强)[1], Zhan-Jun Liu(刘占军)[1,3], Li-Hua Cao(曹莉华)[1,3], and Chun-Yang Zheng(郑春阳)[1,3,†]

[1] *Institute of Applied Physics and Computational Mathematics, Beijing* 100094, *China*

[2] *HEDPS, Center for Applied Physics and Technology, and State Key Laboratory of Nuclear Physics and Technology, School of Physics, Peking University, Beijing* 100871, *China*

[3] *HEDPS, Center for Applied Physics and Technology, and College of Engineering, Peking University, Beijing* 100871, *China*

(Received 20 August 2023; revised manuscript received 17 October 2023; accepted manuscript online 26 October 2023)

A novel scheme to suppress both stimulated Brillouin scattering (SBS) and stimulated Raman scattering (SRS) by combining an alternating frequency (AF) laser and a transverse magnetic field is proposed. The AF laser allows the laser frequency to change discretely and alternately over time. The suppression of SBS is significant as long as the AF difference is greater than the linear growth rate of SBS or the alternating time of the laser frequency is shorter than the linear growth time of SBS. However, the AF laser proves ineffective in suppressing SRS, which usually has a much higher linear growth rate than SBS. To remedy that, a transverse magnetic field is included to suppress the SRS instability. The electrons trapped in the electron plasma waves (EPWs) of SRS can be accelerated by the surfatron mechanism in a transverse magnetic field and eventually detrapped. While continuously extracting energy from EPWs, the EPWs are dissipated and the kinetic inflation of SRS is suppressed. The one-dimensional particle-in-cell simulation results show that both SBS and SRS can be effectively suppressed by combining the AF laser with a transverse magnetic field with tens of Tesla. The total reflectivity can be dramatically reduced by more than one order of magnitude. These results provide a potential reference for controlling SBS and SRS under the related parameters of inertial confinement fusion.

Keywords: stimulated Brillouin scattering, stimulated Raman scattering, alternating frequency laser, transverse magnetic field

PACS: 52.38.–r, 52.38.Bv, 52.57.–z, 52.65.–y **DOI:** 10.1088/1674-1056/ad0716

1. Introduction

Laser plasma instabilities (LPIs), such as stimulated Brillouin scattering (SBS) and stimulated Raman scattering (SRS), are critical issues in the realization of laser-driven inertial confinement fusion (ICF).[1–4] SBS in plasmas is the decay of an incident light wave into a scattered light wave and an ion-acoustic wave (IAW). SRS is the process of incident light wave decay into a scattered light wave and an electron plasma wave (EPW).[5] In these processes, the generation of scattered light can lead to a loss of laser energy. In addition, the potential generation of hot electrons from SRS can lead to target preheating, causing a degradation of compression efficiency and fusion energy gains, both of which are harmful to ignition.[6] Therefore, in studies of laser-driven ICF, the effective management of SRS and SBS at lower levels has always been one of the most important research topics in the field of laser plasma physics. At present, the suppression of LPI is mainly achieved through two approaches: changing the plasma state and improving the incident laser.

In the method of changing the plasma state, on the one hand, the Landau damping of the plasma wave can be enhanced by using filler gases or doping ions to suppress LPI.[7–9] On the other hand, laser plasmas are commonly accompanied by a self-generated magnetic field or an external magnetic field. In recent years, more and more attention has been paid to the effect of magnetic fields on LPIs.[10–21] Montgomery *et al*. pointed out that an external magnetic field of 7.5 T can significantly increase the electron temperature and improve the laser coupling in hohlraum plasmas.[13] Li *et al.* presented a new staged hot-electron acceleration mechanism involving the two-plasmon decay (TPD) instability in the transverse magnetic field and showed that the hot electrons generated by the forward EPW of TPD can be trapped and accelerated again by the backward EPW of TPD, eventually obtaining higher energy.[14] Liu *et al.* studied the effects of an axial magnetic field on the propagation of a linearly polarized laser in plasmas and found that the reflectivity level of SRS was significantly decreased due to the Faraday rotation effect.[15] Pan *et al.* investigated SRS of a left-handed circularly polarized laser in strongly axially magnetized plasmas. The results showed that the external axial magnetic field can not only decrease the linear growth rate and the saturation level of SRS, but also excite SRS instability in over quarter-

†Corresponding author. E-mail: zhengcy@iapcm.ac.cn

© 2024 Chinese Physical Society and IOP Publishing Ltd

critical density plasmas.[16] Winjum and Bailly-Grandvaux *et al.* showed theoretically and experimentally that a transverse magnetic field with tens of Tesla can significantly reduce the reflectivity of SRS in the kinetic regime because the electrons trapped in EPWs propagating perpendicular to a magnetic field can be accelerated by the surfatron mechanism; in addition, the EPWs are strongly damped.[17,18] The research results of Zhou *et al.* indicated that since the nonlinear damping of EPWs is caused by the external transverse magnetic field, the magnetic field can reduce the trapped electrons, limit the kinetic nonlinear frequency shift and narrow the autoresonance region of SRS; thereby, the reflectivity of SRS in inhomogeneous plasma can be effectively controlled.[19]

In the early stages of laser development, a number of strategies for incident laser processing were proposed. They include various laser smoothing technologies, such as random phase plates,[22] continuous phase plates,[23,24] smoothing by spectral dispersion,[25] and polarization smoothing.[26] All these methods or combinations of them have been widely used to control the peak intensities of laser spatial speckles and hence to suppress instabilities in ICF, but they cannot reduce LPIs to a tolerable level.[27,28] Recently, some new theoretical schemes for suppressing LPIs by changing lasers have also been proposed, including various broadband technologies,[29–32] two-color incident light,[33–35] spike trains of uneven duration and delay (STUD),[36–39] rotating polarization,[40–42] alternating polarization,[43,44] the discretely changing phase,[45] etc. It can be seen that in order to reduce the development of LPIs, existing schemes focus on changing the laser frequency, amplitude, polarization direction and phase. These parameters describing the light field can be modulated continuously or discretely. The STUD technique proposed by Afeyan *et al.* transfers laser energy through a short but strong pulse sequence separated by interval periods, which can periodically suspend the interaction time of three waves, thereby reducing the growth of plasma waves and the level of scattered light.[36–39] Liu *et al.* reported the reduction of alternating-polarization light on the scattering levels of SRS and SBS, and the scattering level could be dramatically decreased by more than one order of magnitude under proper alternating-polarization parameters.[43] Yang *et al.* proposed a method in which the phase of incident light was discretely changed. It was shown that the method could broaden the light spectrum and detune the three-wave coupling process; the reflectivity of SRS was observed to decrease significantly.[45] The above three studies correspond to the cases of discretely changing laser amplitude, polarization and phase, respectively. However, the situation of discretely changing frequency remains to be developed.

Moreover, it should be noted that different LPI processes may be simultaneously excited in many ICF experiments. They will gain energy for growth from the incident laser and compete with each other for their own development space. In addition to their competition for the pump laser, there are also other competitive mechanisms. For example, the IAWs excited by SBS can modulate the density of plasmas, which suppresses the development of SRS.[46] The coexistence of SBS and SRS has been observed in many experiments and simulations.[47–51] When attempting to reduce one of the instabilities, it may increase another one, which has an unsatisfactory effect on the overall control of the LPI process. For instance, the suppression of the SBS by a laser with a moderate fractional bandwidth may enhance the SRS and TPD, and then lead to a significant increase in the hot-electron generation.[48] The use of ion doping can improve ion-wave damping, thereby reducing the growth rate of SBS; however, it can also cause difficulties in terms of the development of Langmuir decay instability (which is one of the saturation mechanisms of SRS) and lead to the reflectivity of SRS being maintained at a high level. In some experiments, it has been observed that the level of SRS increases after doping ions.[49,50] In supersonic flowing plasmas, a divergence of plasma flow velocity leads to a strong reduction of the SBS spatial gain and then makes a conducive environment for the growth of SRS, ultimately leading to an increase in the overall reflectivity of the system.[51] Therefore, the competition between SBS and SRS needs further attention and they both need to be suppressed simultaneously in ICF. Solutions to these problems are urgently required.

In this paper, we propose a new theoretical scheme that combines an alternating frequency (AF) laser and a transverse magnetic field to simultaneously suppress both SBS and SRS in laser fusion conditions. This AF laser allows the laser frequency to change discretely and alternately over time. It can suppress SBS and is a useful complement to existing changing laser methods in LPIs. As the AF difference increases and the alternating time decreases, especially when the AF difference is greater than the undamped growth rate γ of SBS or the alternating time is smaller than the undamped growth time $2\pi/\gamma$, the reflectivity of SBS can be reduced markedly. However, the AF laser is ineffective to suppress the SRS that usually has a much higher linear growth rate than the SBS. To remedy that, we also propose to suppress SRS by using an external transverse magnetic field. The EPW propagating perpendicularly to the magnetic field can be damped by the surfatron electron acceleration mechanism. The one-dimensional (1D) particle-in-cell (PIC) simulation results show that the scattering level of both SRS and SBS can be significantly reduced by combining an AF laser and a transverse magnetic field with tens of Tesla.

The paper is structured as follows. In Section 2, the AF laser is introduced. In Section 3, the suppression of SBS using the AF laser is discussed. In Section 4, the simultaneous

suppression of both SBS and SRS is achieved by using the AF laser and a transverse magnetic field in a coexisting SBS–SRS system. The paper is concluded in Section 5.

2. Alternating frequency laser

The schematic diagram and frequency spectrum of the AF light are depicted in Fig. 1. It is composed of two linearly polarized light beams with the same laser intensity but slightly different frequencies, and the two lights are alternated over time. Here, the vacuum wavelengths of these two lights are set to λ_0 and λ_1, corresponding to the orange module and blue module in Fig. 1(a), and their laser periods are T_0 and T_1, respectively. In Fig. 1(a), the AF difference $\Delta f = 1000$ GHz ($\lambda_0 = 0.351$ μm, $\lambda_1 = 0.351411$ μm) and the simulation duration is $6000T_0$ ($T_0 = \lambda_0/c \approx 1.17$ fs, c is the light speed in the vacuum). The laser frequency is changed suddenly for every 200 laser periods, so the alternating period is $200(T_0 + T_1)$.

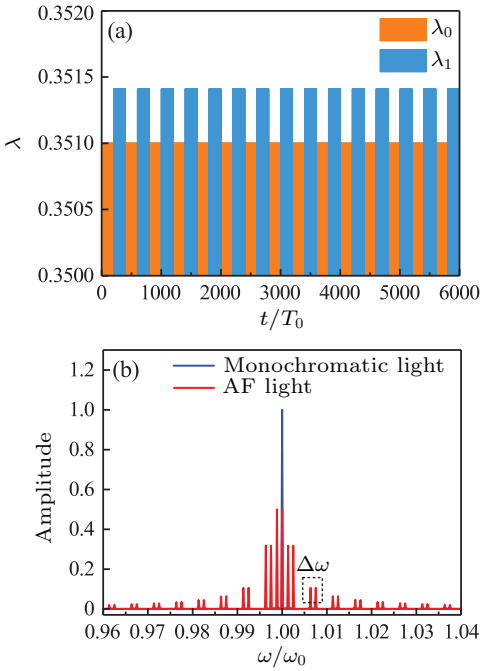


Fig. 1. (a) Schematic diagram of the time evolution of alternating frequency (AF) light. The orange and blue modules represent different wavelengths of light, respectively, and alternate periodically over time. (b) The red and blue solid lines are the spectra of AF light and monochromatic light, respectively. Here, $\lambda_0 = \lambda_m = 0.351$ μm, $\lambda_1 = 0.351411$ μm, the corresponding frequency difference $\Delta f = 1000$ GHz, and the alternating period is $200(T_0 + T_1)$.

The red solid line in Fig. 1(b) is the spectrum of AF laser, while the blue solid line displays the spectrum of monochromatic light ($\lambda_m = \lambda_0 = 0.351$ μm) for comparison. It can be seen that the AF laser spectrum has a certain broadening compared to that of monochromatic light and the laser energy is no longer concentrated on a single frequency but dispersed over the frequency spectrum. In addition, the dispersed frequencies appear in pairs and the difference between each pair of frequencies is equal to that of the given AF laser. As shown in Fig. 1(b), $\Delta\omega = 0.117\%\ \omega_0$ (ω_0 is the angular frequency of light with λ_0), the corresponding $\Delta f = 1000$ GHz is the same as the frequency difference of AF light in Fig. 1(a). This AF laser can be the combination of two STUD lasers for a single beam[52] and there is no need to increase the intensity of the incident laser to avoid optical damage when using high power lasers compared to the STUD laser.

3. Supperssion of SBS by alternating frequency laser

In this paper, we mainly carry out 1D numerical simulations via the PIC code EPOCH.[53] The influence of an AF laser on SBS is investigated in this section. Referring to the physical parameters in the ICF experiments, the plasma density is set to $n_e = 0.06\ n_c$, where n_c ($n_c \equiv 1.11 \times 10^{21}/\lambda^2_{0,\mu m}$ in cm^{-3}) denotes the critical density of the 3ω light. The plasma is homogeneous, collisionless and in equilibrium at the beginning. The initial electron and He ion temperatures are $T_e = 1.5$ keV and $T_i = 0.3$ keV, respectively. The ion charge $Z = 2$ and the ion mass $m_i = 7344\ m_e$ (m_e is the electron mass); it can be calculated that $ZT_e/T_i = 10$. The wavelengths of two p-polarized light beams in AF lasers are λ_0 and λ_1, respectively. For convenience, $\lambda_0 = 0.351$ μm remains unchanged in the simulation, the selected range of λ_1 is around 0.351 μm–0.352 μm. The simulation box is $L = 680\ \lambda_0$ and divided into 28646 cells (120 cells per micron), there are 600 electrons and 400 He ions per cell at the initial time. The total simulation time is $20000T_0 \approx 23.4$ ps and the alternating period of the AF laser is between $100(T_0 + T_1)$ and $6000(T_0 + T_1)$. The intensities of these two lights are all $I_{0,1} = 6.0 \times 10^{14}$ W/cm^2 and the normalized vector potential $a_0 = eE_0/(m_e\omega_0 c) = 0.0073$ (e denotes the electron charge), which alternately enter the box from the left boundary and propagate along the x-direction. At the same time, the corresponding seed light also alternately comes from the right boundary with the intensity $I_{s0,1} = 1/500\ I_{0,1}$ to quickly excite SBS. The wavelength $\lambda_{s0,1}$ of seed light ($\lambda_{s0} = 0.35168$ μm for $\lambda_0 = 0.351$ μm) is given from the three-wave matching condition $\boldsymbol{k}_{0,1} = \boldsymbol{k}_{s0,1} + \boldsymbol{k}_{i0,1}$ and $\omega_{0,1} = \omega_{s0,1} + \omega_{i0,1}$, where the subscripts 0/1, s0/s1 and i0/i1 represent the pump, scattering (seed) and ion acoustic wave, respectively. The dispersion relations of different modes are $\omega^2_{0,s0} = \omega^2_{pe} + c^2k^2_{0,s0}$, $\omega^2_{i0} = c_s^2k^2_{i0}$, where $\omega_{pe} = \sqrt{4\pi n_e e^2/m_e}$ is the plasma frequency, $c_s = \sqrt{(ZT_e + 3T_i)/m_i}$ is the ion acoustic velocity. The thermal boundaries for particles and the absorbing boundaries for fields are used in the simulation.

With the above plasma and laser parameters, the undamped growth rate of SBS for the monochromatic light ($\Delta f = 0$) is $\gamma = k_i v_{os}\omega_{pi}/(4\sqrt{\omega_0 k_i c_s}) \approx 3.2 \times 10^{-4}\omega_0$, where v_{os} is the oscillating velocity of the electron in the driven laser and ω_{pi} is the ion plasma frequency. The Landau damping rate

of the IAW $\nu_{\rm iaw} \approx 6.2\times10^{-5}\omega_0$. In this case, SBS can be excited significantly. By performing a fast Fourier transform on the longitudinal electric field, the dispersion relation of the E_x field is obtained in Fig. 2(a1) corresponding to the monochromatic light, which shows the SBS is dominant in the system. By using three-wave matching conditions, it can be calculated that the frequency of the IAW is $\omega_{\rm iaw} = 1.93\times10^{-3}\omega_0$, which is also consistent with the simulation results. The blue solid line in Fig. 2(b) represents the temporal evolution of the SBS reflectivity (measured from the left boundary of the simulation box) for the monochromatic light, corresponding to the same parameters in Fig. 2(a1). From Fig. 2(b), the linear growth and saturation stage for the scattered light of SBS can be clearly observed. In the growth interval, its linear growth time is about $4000T_0$. At this time, the IAW grows to a large amplitude and begins to trap the ions, which leads to the nonlinear frequency shift of the IAW. Then, the SBS is no longer growing rapidly and begins to saturate. The reflectivity of SBS is about 25% when it reaches its peak at around $8000T_0$ and then enters the nonlinear saturation stage.

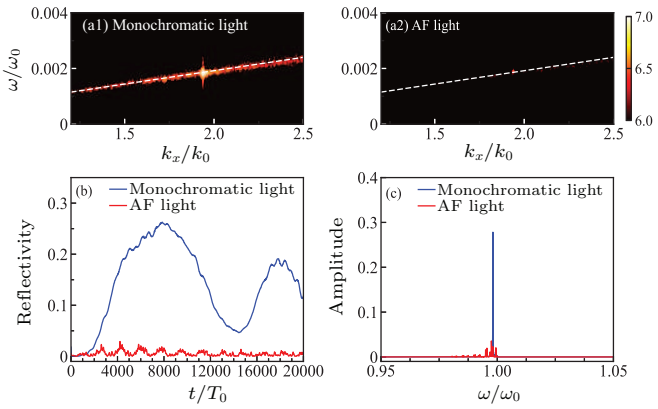


Fig. 2. (a1) and (a2) Plots of the dispersion relation for the longitudinal electric field. The white dotted lines represent the dispersion relation of IAWs. The colorbars for (a1) and (a2) are in arbitrary units. (b) Evolution of reflectivity for SBS at the left boundary. (c) Frequency spectrum corresponding to (b). The frequency difference of AF light is $\Delta f = 500$ GHz and the alternating period is $200(T_0+T_1)$.

Figure 2(a2) shows the spectrum map of the IAW with the AF difference 500 GHz and an alternating period $200(T_0+T_1)$. It can be seen that the intensity of the IAW in Fig. 2(a2) is prominently weakened compared to Fig. 2(a1). The corresponding evolution of reflectivity is shown by the red solid line in Fig. 2(b). It is shown that for the AF laser, the reflectivity of SBS is controlled at an extremely low level, which means that SBS is not significantly excited during the entire process. For this case in Fig. 2(b), the undamped growth time for monochromatic light is about $t_{\rm g} = 2\pi/\gamma = 3125T_0$ and the alternating time for the AF light is about $200T_0$. When the alternating time is shorter than the undamped growth time, the frequency of the laser is changed before SBS has grown sufficiently and the SBS that occurred in the previous period is unable to effectively couple in the new stage. This method can break the three-wave matching of SBS, reduce the laser plasma interaction time and disrupt the sustained growth of instability, as shown in Fig. 2(b). Moreover, it can also be seen from the frequency spectra of the reflectivity [as shown in Fig. 2(c)] that when using the AF laser, the amplitude obviously decreases and the spectrum widens slightly.

By comparing the monochromatic and AF light in Fig. 2, it is clear that the AF laser can effectively suppress SBS in both linear and nonlinear stages.

Figures 3(a1) and 3(a2) show the spatial evolutions of IAWs under monochromatic and AF light, respectively. From Fig. 3(a1), it can be seen that a strong IAW can be excited in the plasmas and the density perturbations of the IAW gradually increase with time. In contrast, for the AF laser, there is no significant ion acoustic disturbance in the plasma and no fluctuation over time [see Fig. 3(a2)]. By performing Fourier transform on Figs. 3(a1) and 3(a2) in the space, the corresponding wavenumber spectrum of the IAWs can be obtained in Figs. 3(b1) and 3(b2). The wave number region of the IAW for the monochromatic light in Fig. 3(b1) is wide and it has large amplitude. The ions will be trapped when the IAW grows to a large amplitude, resulting in a nonlinear frequency shift of the IAW. However, the IAW amplitude evidently decreases after the SBS is suppressed by the AF light in Fig. 3(b2). The nonlinear frequency shift no longer occurs and the spectral width becomes very narrow. The above results indicate that the AF laser can suppress the instability growth of SBS.

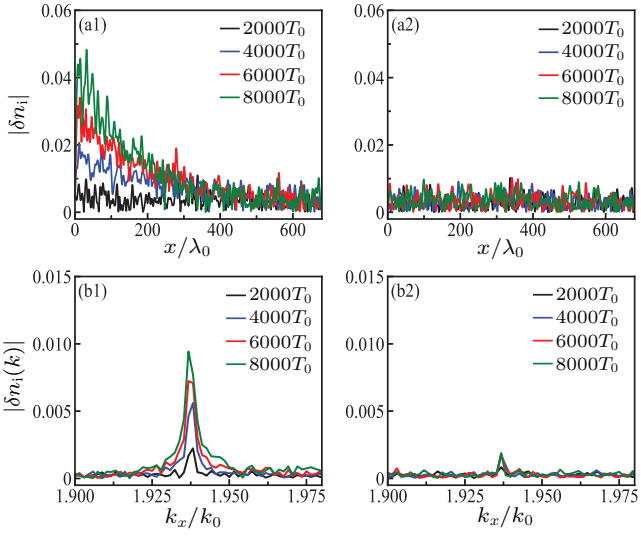


Fig. 3. (a1) and (a2) Spatial evolutions of the ion density disturbance for the monochromatic light and AF light, respectively, at different times. Here $\delta n_{\rm i} = (n_{\rm i} - n_{\rm i0})/n_{\rm i0}$. (b1) and (b2) Wavenumber spectrum of the ion density disturbance corresponding to (a1) and (a2). In (a1) and (b1), $\Delta f = 0$ GHz. In (a2) and (b2), $\Delta f = 500$ GHz and the alternating period is $200(T_0+T_1)$.

Figure 4 shows the effects of the AF laser on the time-averaged reflectivity of SBS with different parameters. The results indicate that the AF laser has sufficiently suppressed

SBS. In Fig. 4(a), we investigate the variation of SBS reflectivity as a function of the AF difference for a fixed alternating period of $2000(T_0+T_1)$. It is found that because the alternating time here is shorter than the undamped growth time t_g of SBS, even if there is a small frequency difference (such as 50 GHz) in the AF laser, a certain suppression effect on SBS can also be achieved. The SBS reflectivity decreases as the AF difference increases. Specially, when the AF difference is greater than the SBS growth rate $\gamma = 3.2\times10^{-4}\omega_0$ [the corresponding frequency is 273.5 GHz, see the dashed line in Fig. 4(a)], the suppression effect on SBS is significantly enhanced and then gradually stabilizes as it continues to increase the AF difference.

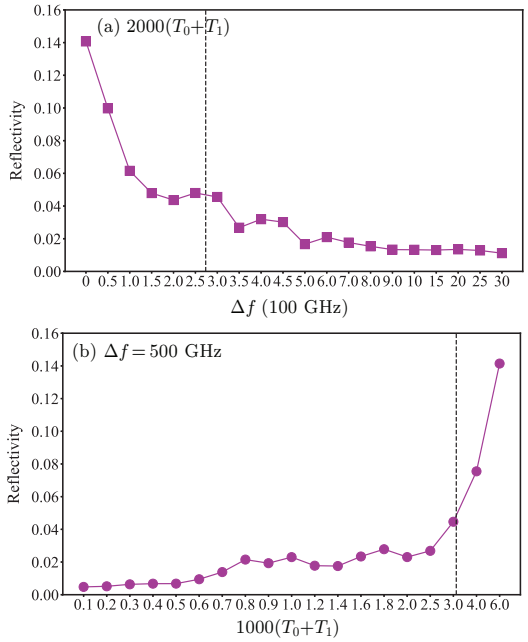


Fig. 4. The impact of the different AF light on SBS reflectivity. (a) Time-averaged reflectivity of SBS for different frequency differences with the alternating period $2000(T_0+T_1)$. (b) Time-averaged reflectivity of SBS for different alternating periods with $\Delta f = 500$ GHz.

Figure 4(b) plots the variation of SBS reflectivity with different alternating periods for the fixed AF difference $\Delta f =$ 500 GHz, which is greater than the undamped growth rate of SBS. It can be seen that as the alternating period decreases, the scattering level of the SBS can be significantly reduced. Specifically, an obvious decreasing SBS for the AF laser is observed when the alternating time is less than the undamped growth time [calculated by $2\pi/\gamma = 3125T_0$, corresponding to the dashed line in Fig. 4(b)], and the level of scattered light can be dramatically reduced by more than one order of magnitude. As the alternating time is greater than the undamped growth time, the suppression on SBS becomes less obvious and the scattering level tends towards the case of monochromatic light gradually. Due to the fact that the growth rate of SRS is much higher than that of SBS, the impact of the AF laser on SBS is much more sensitive than that of SRS. Of course, the AF laser still limits the development of SRS when the AF difference is large enough, especially when the AF difference is greater than the growth rate of SRS. We have already verified the results and do not delve into a discussion here. In brief, this section has demonstrated that the AF laser has a significant suppression effect on SBS.

4. Simultaneous suppression of SBS and SRS by the alternating frequency laser and transverse magnetic field

In many experiments and simulations, the coexistence of SBS and SRS has been observed, and they may compete and influence each other. Generally, taking a single measure to reduce one instability may actually increase another, resulting in an unsatisfactory overall effect.[47–51] Therefore, both SBS and SRS need to be suppressed as much as possible in ICF. In this section, we propose a theoretical scheme that combines AF light and a transverse magnetic field to simultaneously suppress SBS and SRS. Firstly, the impact of a transverse weak magnetic field (less than 100 T) on SRS is investigated, as shown in Fig. 5. Here, the selection of physical parameters is as follows. The initial temperatures of the electron and the He ion are set to $T_e = 1.2$ keV, $T_i = 0.6$ keV. To focus on the SRS instability, the He ions are immobile in this case.

The intensity of the incident laser is $I_0 = 1.2\times10^{15}$ W/cm^2 and the corresponding seed light intensity is 1/500 of the incident light. The wavelength of seed light is given from the three-wave matching condition, which gives $\lambda_s = 0.4955$ μm, and the total simulation time is $5000T_0$. Here, the dimensionless parameter $k_l\lambda_d = 0.3255$, where k_l is the Langmuir wavenumber and λ_d is the Debye length. These parameters are chosen in the kinetic region and the wave–particle coupling is important. The other parameters are consistent with the previous section.

Figure 5 shows the influence of the transverse magnetic field on SRS. Figures 5(a1) and 5(a2) correspond to the unmagnetized case, while Figs. 5(b1) and 5(b3) correspond to the magnetized case. The evolution of SRS reflectivity in these two cases is displayed in Fig. 5(c). The transverse magnetic field in Fig. 5 is $B_z = 60$ T, the electron cyclotron frequency $\omega_c = 1.96\times10^{-3}\omega_0$ ($\omega_c/\omega_0 \ll 1$) and the influence of an external magnetic field on the dispersion relations of electromagnetic waves and EPWs is negligible.[19] The spectrum signal of SRS with $B_z = 0$ T is shown in Fig. 5(a1). There are the obvious backward scattering and weak forward scattering signals for SRS. The white dashed line represents the dispersion relation of the Langmuir wave $\omega_l^2 = \omega_{pe}^2(1+3k_l^2\lambda_d^2)$ and the wave numbers of the forward scattering and backward scattering are $k_{l-f} = 0.256\,k_0$ and $k_{l-b} = 1.645\,k_0$, respectively. Furthermore, the EPW has a significant nonlinear frequency shift, which is induced by the electron trapping. The clear electron

trapping structure can also be seen from Fig. 5(a2) in p_x–x space at $t = 2400T_0$. In the kinetic regime ($k_1\lambda_d = 0.3255$), the electron trapping effect can significantly reduce the Landau damping and if it exceeds the kinetic inflation threshold, the SRS reflectivity will reach a very high level, as shown by the blue solid line in Fig. 5(c).

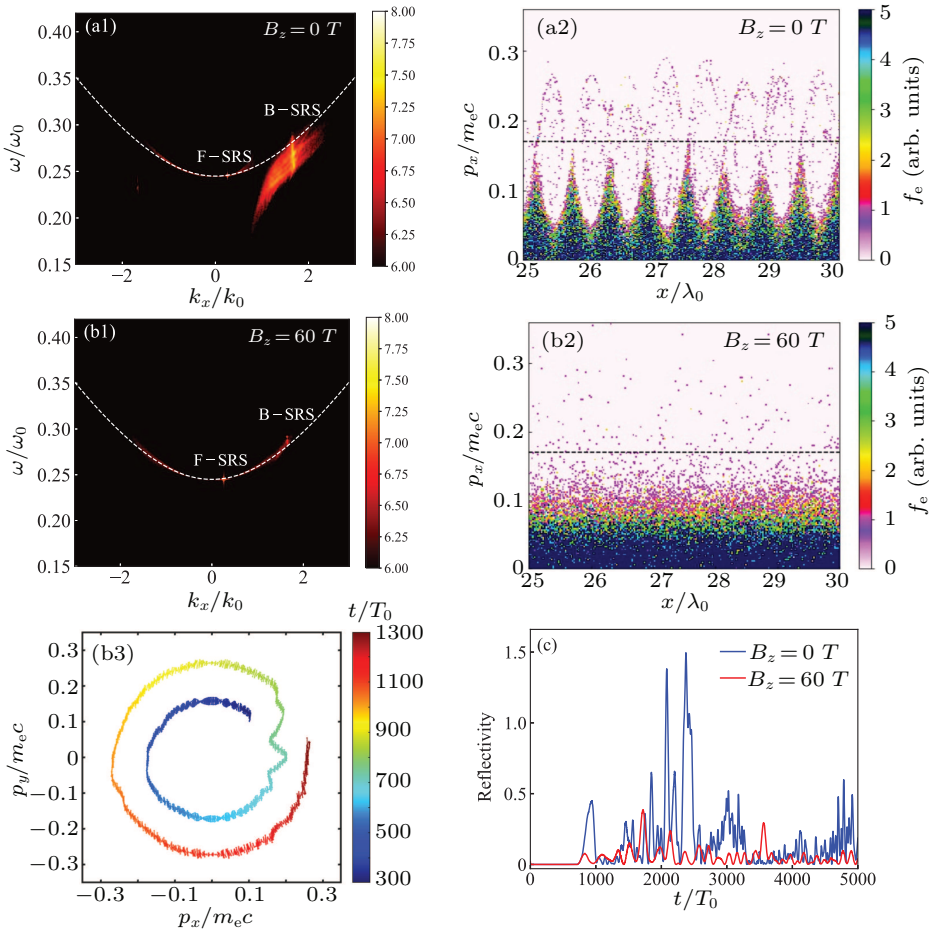


Fig. 5. (a1) and (b1) Plots of the dispersion relation for the longitudinal electric field; the white dashed lines represent the dispersion relation of EPWs. The colorbars for (a1) and (b1) are in arbitrary units. (a2) and (b2) Electron distribution in p_x–x space at $t = 2200T_0$; the black dashed lines denote the phase velocity of the prime EPWs. (b3) The track of one electron in p_x–p_y space over $t = 300T_0$–$1300T_0$. (c) The evolution of reflectivity for SRS at the left boundary. In (a1) and (a2), $B_z = 0$ T. In (b1)–(b3), $B_z = 60$ T.

When considering an external transverse magnetic field, the results indicate that it has a significant suppression on SRS. As shown in Fig. 5(b1), the amplitude of the EPW is obviously weakened and the electron trapping-induced nonlinear frequency shift is also limited. Compared with Fig. 5(a2), in the external magnetic field, Fig. 5(b2) exhibits that the trapped electrons can escape from the potential well and eventually detrap. In addition, the kinetic inflation of SRS is also suppressed [see the red solid line in Fig. 5(c)]. Essentially, the electrons trapped around the EPW phase velocity v_{ph} can be accelerated perpendicularly across the wavefront by the surfatron mechanism, continuously extracting energy from the wave, and meanwhile the EPWs are heavily damped.[54,55] This is also the fundamental reason for suppressing SRS. Figure 5(b3) shows the track of one electron trapped by the EPW in p_x–p_y space over $t = 300T_0$–$1300T_0$ under an external magnetic field. It can be seen that the trapped electron has a longitudinal oscillation near the phase velocity ($v_{ph} = 0.17\ c$); meanwhile it is accelerated in the transverse direction. Eventually the particle detraps after accelerating to the escape speed and then continues executing cyclotron motion in p_x–p_y space.[19]

In addition, the forward SRS is slightly enhanced in the external magnetic field, as shown in Fig. 5(b1). The phase velocity of the forward SRS ($v_{ph} = 0.959\ c$) is very large; thus, the number of electrons trapped by EPWs is small and the nonlinear damping caused by the magnetic field has almost no effect on it. Due to the competition for the pump light, the backward SRS weakens and the forward SRS increases. For SBS, the phase velocity of the IAW is very small and far lower than the phase velocity of the Langmuir wave. The efficiency of the energy loss for the electrostatic wave caused by the nonlinear damping is proportional to the phase velocity. The force perpendicularly across the wavefront felt by the ions trapped in IAWs is very small, so they cannot effectively obtain energy from the wave.[54,55] Therefore, it is difficult to reflect the nonlinear damping caused by the external magnetic field on IAWs,

leading to no suppression of SBS.

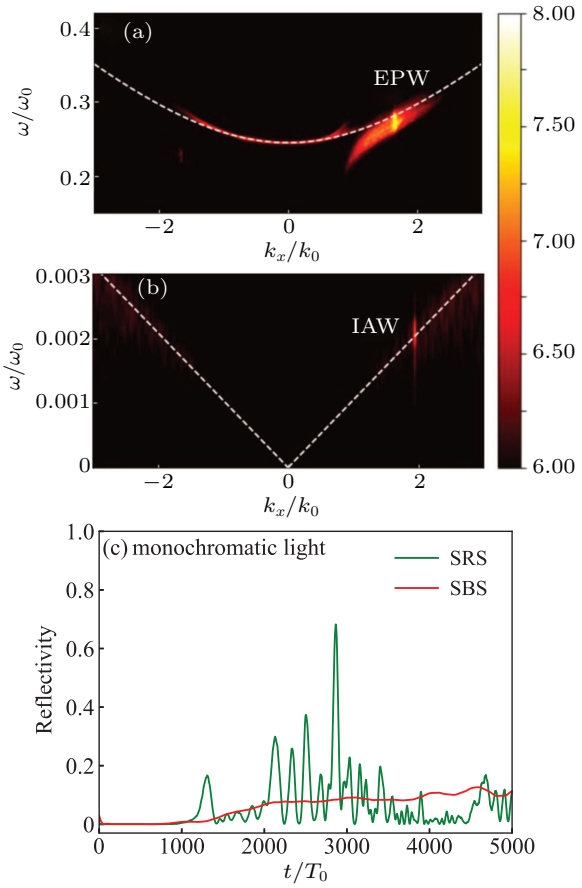


Fig. 6. (a) and (b) Plots of the dispersion relation for the longitudinal electric field; the white dashed lines in (a) and (b) represent the dispersion relation of EPW and IAW in plasmas, respectively. The colorbars for (a) and (b) are in arbitrary units. (c) The evolution of reflectivity at the left boundary.

Based on the above analysis, utilizing the sensitivity of SBS to the AF laser and the sensitivity of SRS to the magnetic fields, we propose a theoretical scheme combining the AF laser and the transverse magnetic field to simultaneously suppress SBS and SRS. Next, we will adopt the parameter settings in Fig. 5 except that the ions are mobile. It is noted that due to the small growth rate of SBS and the limitation of simulation time, only the seed light of SBS is given here to quickly excite SBS ($\lambda_s = 0.35175$ μm) in the simulation and then reduce the time required for SBS growth. We first show the dispersion relation of the longitudinal electric field in Figs. 6(a) and 6(b) when the AF laser is not used and there is no external magnetic field. It is obtained by performing a fast Fourier transform on the longitudinal electric field with the entire time and space domain. It is clearly seen as the coexistence of SRS and SBS. Due to the different frequency ranges and significant differences in the scattered light of SBS and SRS, the evolution of their own reflectivity can be obtained separately through filtering, as shown in Fig. 6(c). It can be calculated that the time-averaged reflectivity of SBS is 6.07% and that of SRS is 6.26%; so, SBS and SRS have comparable levels in the system. The SRS develops before SBS and there is a kinetic inflation behavior (here $k_l\lambda_d = 0.3255$). Subsequently, SBS also grows with time and the IAWs can excite a density modulation in the plasma. Due to the density modulation and the pump depletion, the reflectivity of SRS decreases when SBS increases. This indicates that there is a competitive relationship between them.

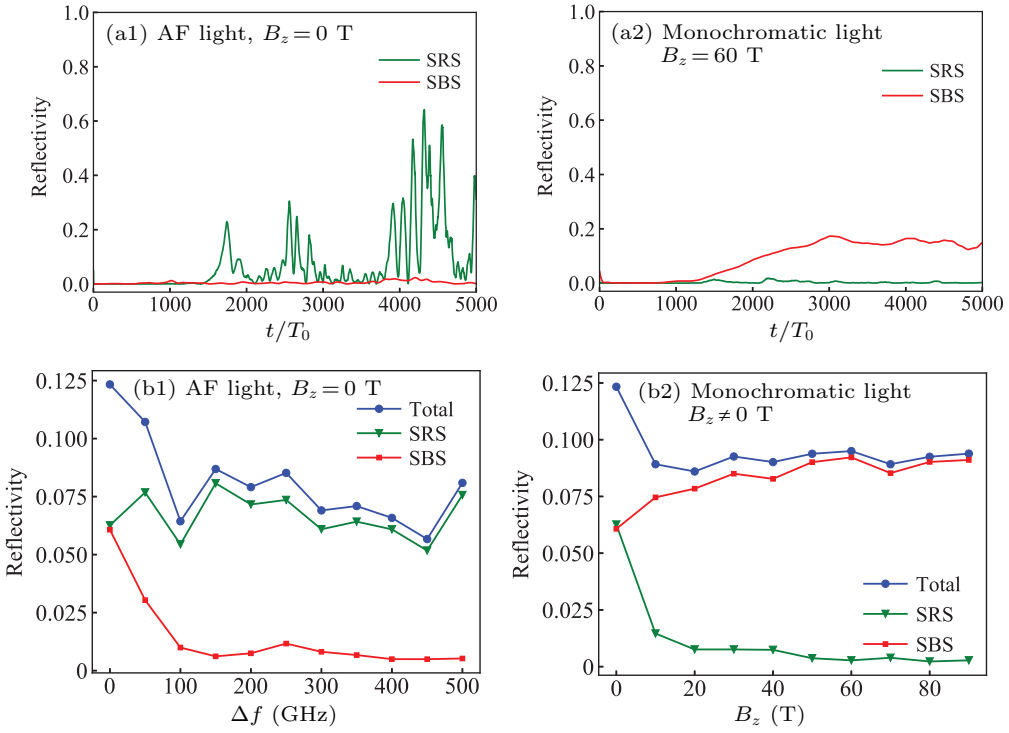


Fig. 7. The time evolution (a1) and (a2) and the time average (b1) and (b2) of SBS and SRS reflectivity for different AF lights and magnetic fields. (a1) and (b1) $B_z = 0$ T, the alternating period is $200(T_0 + T_1)$, and $\Delta f = 500$ GHz in (a1). (a2) and (b2) $\Delta f = 0$ GHz and $B_z = 60$ T in (a2).

The effect of the AF laser on the reflectivity of SBS and SRS without an external magnetic field is investigated in this system. In Fig. 7(a1), the alternating period of the AF laser is $200(T_0+T_1)$, the frequency difference is 500 GHz and the growth rate of SBS is $\gamma = 4.47\times10^{-4}\omega_0$. Where $200T_0$ is less than the undamped growth time of SBS ($t_g = 2\pi/\gamma = 2237T_0$) and 500 GHz is also greater than the growth rate of SBS ($\gamma = 4.47\times10^{-4}\omega_0 = 382$ GHz). According to the analysis in the previous section, this AF laser has a good suppression effect on SBS. By comparing Figs. 7(a1) and 6(c), the time-averaged SBS reflectivity decreased from 6.07% to 0.52% and the scattering level is dramatically reduced by one order of magnitude. However, the reflectivity of SRS does not decrease and even increases in the later stage due to pump competition. Eventually, the total time-average reflectivity of the system only decreases from 12.3% to around 8.1%. Figure 7(b1) shows the time-averaged reflectivity of the system (including SBS, SRS and total) for different AF differences with the fixed alternating period $200(T_0+T_1)$. The reflectivity of SBS significantly reduces first and then stabilizes at a lower level as the frequency difference increases. The SRS reflectivity oscillates slightly at the initial level and eventually slightly increases. Therefore, the overall reflectivity has not decreased significantly.

As a comparison, Figs. 7(a2) and 7(b2) also provide the situation when there is only an external transverse magnetic field. It can be seen that the reflectivity of SRS is very sensitive to the transverse magnetic field, as mentioned above. Although SRS is suppressed dramatically (from 6.26% to 0.28%), SBS clearly increases [see the red solid lines in Figs. 7(a2) and 6(c)], resulting in no significant decrease of the total scattering level (from 12.3% to 9.5%). The effects of the magnetic field on the time-averaged scattering level are shown in Fig. 7(b2). The reflectivity of SRS can be reduced remarkably with a magnetic field of only about 20 T. Under the influence of the transverse magnetic field, while the reflectivity of the SRS decreases, the SBS reflectivity increases obviously. The total scattering level still remains high for this situation. Note that when the SRS reflectivity is at a lower level, the reflectivity of SBS hardly fluctuates with the increase of the external magnetic field, which is also evidence that the transverse magnetic field has little influence on SBS.

Figure 8 shows the simulation results when the AF laser and the transverse external magnetic field are used simultaneously. In Fig. 8(a), the AF difference is $\Delta f = 500$ GHz, the alternating period is $200(T_0+T_1)$ and the magnetic field is $B_z = 60$ T. It can be clearly seen that, in this situation, both SBS and SRS can be reduced to very low levels, resulting in a significant decrease from 12.3% to 0.8% of the total reflectivity. In addition, due to the external magnetic field limiting the nonlinear frequency shift of SRS and narrowing the spectrum of SRS, the AF laser in magnetized plasmas has a slightly greater impact on SRS, than that in unmagnetized plasmas. Figure 8(b) illustrates the time-averaged reflectivity of the system for different AF differences when the alternating period and magnetic field are fixed at $200(T_0+T_1)$ and 60 T, respectively. It can be seen that the reflectivity of SRS is always at a low level under the impact of the magnetic field. The SBS reflectivity decreases remarkably with the increase of the frequency difference and subsequently remains at a lower level. The result is that the total scattering level of the system can be dramatically reduced by more than one order of magnitude. The above simulation results demonstrate that both SBS and SRS can be suppressed by combining an AF laser and a transverse external magnetic field.

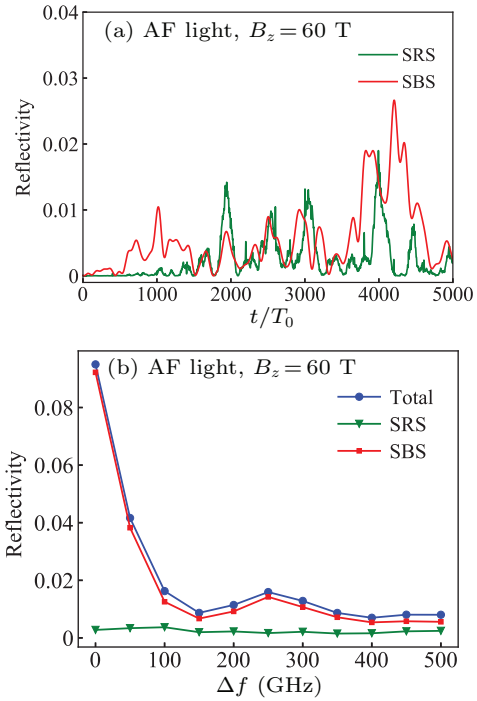


Fig. 8. (a) The time evolution of SBS and SRS reflectivity for an AF light and a fixed magnetic field. (b) The time-averaged SBS and SRS reflectivity for different AF lights and a fixed magnetic field. (a) and (b) $B_z = 60$ T, the alternating period is $200(T_0+T_1)$, and $\Delta f = 500$ GHz in (a).

5. Conclusions

In summary, with the help of 1D PIC simulation, we investigate the suppression of SBS and SRS by using an AF laser and a transverse magnetic field. A new method for reducing the SBS is proposed by using the AF laser. This method alternately changes the laser frequency through time modulation, which can break the three-wave matching process of SBS and then reduce SBS. As the alternating period decreases and the AF difference increases, the suppression effects on SBS become apparent. Especially, if the alternating time is less than the undamped growth time of SBS and the AF difference is greater than its growth rate, the reduction of SBS becomes gradually significant. Due to the fact that the growth rate of SRS is much higher than that of SBS, the impact of the AF laser on SBS is much more sensitive than that of SRS. In addition, the coexistence of SRS and SBS has often been observed

in simulations and experiments, and they may compete and influence each other. Usually, when using a single method to suppress one instability, another instability may increase due to pump competition, resulting in unsatisfactory suppression in the LPI. Based on the sensitivity of SBS to AF light, combined with the characteristic that a transverse magnetic field suppresses SRS while SBS is not sensitive to it, we propose a theoretical scheme for simultaneously suppressing SBS and SRS that combines AF light with an external transverse magnetic field. The results show that both SBS and SRS are significantly suppressed after adopting this scheme and that the scattering levels of SBS and SRS are dramatically reduced, allowing the total reflectivity to be at a low level. Specifically, when only the AF laser or the magnetic fields are considered, although they can reduce SBS and SRS separately and dramatically, the total reflectivity of the system only decreases from 12.3% to 8.1% and 9.5%. By combining the two methods, the total reflectivity of the system is directly reduced from 12.3% to 0.8% by more than one order of magnitude.

Acknowledgement

Project supported by the National Natural Science Foundation of China (Grant Nos. 11975059 and 12005021).

References

[1] He X T, Li J W, Fan Z F, Wang L F, Liu J, Lan K, Wu J F and Ye W H 2016 *Phys. Plasmas* **23** 082706
[2] Hinkel D E, Rosen M D, Williams E A, Langdon A B, Still C H, Callahan D A, Moody J D, Michel P A, Town R P J, London R A and Langer S H 2011 *Phys. Plasmas* **18** 056312
[3] Tikhonchuk V T, Gong T and Jourdain N, *et al.* 2021 *Matter Radiat. Extremes* **6** 025902
[4] Liu Z J, Wang Q, Li B, Li J W, Cao L H, Zheng C Y and He X T 2022 *Plasma Phys. Control. Fusion* **64** 035002
[5] Kruer W L 1988 *The Physics of Laser Plasma Interactions* (Addison-Wesley Publishing Company)
[6] Dewald E L, Hartemann F, Michel P, *et al.* 2016 *Phys. Rev. Lett.* **116** 075003
[7] Hinkel D E, Edwards M J and Amendt P A, *et al.* 2013 *Plasma Phys. Control. Fusion* **55** 124015
[8] Feng Q S, Zheng C Y, Liu Z J, Cao L H, Wang Q, Xiao C Z and He X T 2019 *Phys. Plasmas* **26** 052101
[9] Froula D H, Divol L, London R A, Berger R L, Döppner T, Meezan N B, Ross J S, Suter L J, Sorce C and Glenzer S H 2009 *Phys. Rev. Lett.* **103** 045006
[10] Stamper J A, Papadopoulos K, Sudan R N, Dean S O, McLean E A and Dawson J M 1971 *Phys. Rev. Lett.* **26** 1012
[11] Farmer W A, Koning J M, Strozzi D J, Hinkel D E, Berzak Hopkins L F, Jones O S and Rosen M D 2017 *Phys. Plasmas* **24** 052703
[12] Zhou Y Z, Zheng C Y, Liu Z J and Cao L H 2022 *Plasma Phys. Control. Fusion* **64** 045009
[13] Montgomery D S, Albright B J, Barnak D H, Chang P Y, Davies J R, Fiksel G, Froula D H, Kline J L, MacDonald M J, Sefkow A B, Yin L and Betti R 2015 *Phys. Plasmas* **22** 010703
[14] Li X X, Cheng R J, Wang Qing, Liu D J, Lv S Y, Huang Z M, Zhang S T, Li X M, Chen Z J, Wang Qiang, Liu Z J, Cao L H, Zheng C Y and He X T 2023 *Phys. Rev. E* **108** L053201
[15] Liu Z J, Li B, Xiang J, Cao L H, Zheng C Y and Hao L 2018 *Plasma Phys. Control. Fusion* **60** 045008
[16] Pan K Q, Guo L, Li Z C, Yang D, Li S W, Jiang S E, Zhang B H, Zheng C Y and He X T 2019 *Phys. Plasmas* **26** 012108
[17] Winjum B J, Tsung F S and Mori W B 2018 *Phys. Rev. E* **98** 043208
[18] Bailly-Grandvaux M, Winjum B J, Manuel M J E, Bolaños S, Walsh C A, Saret J, Bogale J, Strehlow J, Lee R, Tsung F, Mori W, Froula D H, Filkins T and Beg F N 2023 *J. Plasma Phys.* **89** 175890201
[19] Zhou Y Z, Zheng C Y, Liu Z J and Cao L H 2021 *Plasma Phys. Control. Fusion* **63** 055015
[20] Shi Y, Qin Hong and Fisch N J 2018 *Phys. Plasmas* **25** 055706
[21] Edwards M R, Shi Y, Mikhailova J M and Fisch N J 2019 *Phys. Rev. Lett.* **123** 025001
[22] Moody J D, MacGowan B J, Rothenberg J E, Berger R L, Divol L, Glenzer S H, Kirkwood R K, Williams E A and Young P E 2001 *Phys. Rev. Lett.* **86** 2810
[23] Dixit S N, Feit M D, Perry M D and Powell H T 1996 *Opt. Lett.* **21** 001715
[24] Zhang R, Jia H T, Tian X C, Yuan H Y, Na Z, Su J Q, Hu D X, Zhu Q H and Zheng W G 2016 *Opt. Lasers Eng.* **85** 38
[25] Skupsky S, Short R W, Kessler T, Craxton R S, Letzring S and Soures J M 1989 *J. Appl. Phys.* **66** 3456
[26] Lefebvre E, Berger R L, Langdon A B, MacGowan B J, Rothenberg J E and Williams E A 1998 *Phys. Plasmas* **5** 2701
[27] Moody J D, MacGowan B J, Rothenberg J E, Berger R J, Divol L, Glenzer S H, Kirkwood R K, Williams E A and Young P E 2001 *Phys. Rev. Lett.* **86** 2810
[28] Mounaix Ph, Divol L, Hüller S and Tikhonchuk V T 2000 *Phys. Rev. Lett.* **85** 4526
[29] Ma H H, Li X F, Weng S M, Yew S H, Kawata S, Gibbon P, Sheng Z M and Zhang J 2021 *Matter Radiat. Extremes* **6** 055902
[30] Follett R K, Shaw J G, Myatt J F, Wen H, Froula D H and Palastro J P 2021 *Phys. Plasmas* **28** 032103
[31] Zhao Y, Weng S M, Chen M, Zheng J, Zhuo H B, Ren C, Sheng Z M and Zhang J 2017 *Phys. Plasmas* **24** 112102
[32] Luo M F, Hüller S, Chen M and Sheng Z M 2022 *Phys. Plasmas* **29** 032102
[33] Liu Z J, Chen Y H, Zheng C Y, Cao L H, Li B, Xiang J, Hao L and Lan K 2017 *Phys. Plasmas* **24** 082704
[34] Feng Q S, Liu Z J, Cao L H, Xiao C Z, Hao L, Zheng C Y, Ning C and He X T 2020 *Nucl. Fusion* **60** 066012
[35] Wang Q, Li Z C and Liu Z J, *et al.* 2023 *Matter Radiat. Extremes* **8** 055602
[36] Albright B J, Yin L and Afeyan B 2014 *Phys. Rev. Lett.* **113** 045002
[37] Afeyan B and Hüller S 2013 *Eur. Phys. J. Web Conf.* **59** 05009
[38] Hüller S and Afeyan B 2013 *Eur. Phys. J. Web Conf.* **59** 05010
[39] Yin L, Albright B J, Rose H A, Montgomery D S, Kline J L, Kirkwood R K, Milovich J, Finnegan S M, Bergen B and Bowers K J 2014 *Phys. Plasmas* **21** 092707
[40] Barth I and Fisch N J 2016 *Phys. Plasmas* **23** 102106
[41] Zhou H Y, Xiao C Z, Jiao J L, Lang Y, Zhao N, Xie D, Zou D B, Yin Y, Shao F Q and Zhuo H B 2019 *Plasma Phys. Control. Fusion* **61** 105004
[42] Ban S S, Wang Q, Liu Z J, Zheng C Y and He X T 2020 *Chin. Phys. B* **29** 095202
[43] Liu Z J, Zheng C Y, Cao L H, Li B, Xiang J and Hao L 2017 *Phys. Plasmas* **24** 032701
[44] Liu Z J, Wang Q, Zhang W S, Li B, Li P, Zheng W G, Li X, Li J W, Cao L H, Zheng C Y, Ding Y K and He X T 2023 *Phys. Plasmas* **30** 032703
[45] Yang T, Zhang S T, Zhou Y Z, Liu D J, Li X M, Liu Z J, Cao L H, Zheng C Y and He X T 2021 *Phys. Scr.* **96** 125634
[46] Zhang H C, Xiao C Z, Wang Q, Feng Q S, Liu Z J and Zhen C Y 2017 *Phys. Plasmas* **24** 032118
[47] Klimo O, Weber S, Tikhonchuk V T and Limpouch J 2010 *Plasma Phys. Control. Fusion* **52** 055013
[48] Liu Z, Ma H H, Wang W, Li X F, Wang P P, Wang C, Yew S H, Weng S M, Sheng Z M and Zhang J 2023 *Nucl. Fusion* **63** 126010
[49] Fernández J C, Cobble J A, Failor B H, DuBois D F, Montgomery D S, Rose H A, Vu H X, Wilde B H, Wilke M D and Chrien R E 1996 *Phys. Rev. Lett.* **77** 2702
[50] Kirkwood R K, MacGowan B J, Montgomery D S, Afeyan B B, Kruer W L, Moody J D, Estabrook K G, Back C A, Glenzer S H, Blain M A, Williams E A, Berger R L and Lasinski B F 1996 *Phys. Rev. Lett.* **77** 2706
[51] Shekhanov S A and Tikhonchuk V T 2021 *Plasma Phys. Control. Fusion* **63** 115016
[52] Li Y, Wang S W, Xu J Q and Tang Y L 2015 *Opt. Express* **23** 029484
[53] Arber T D, Bennett K, Brady C S, Lawrence-Douglas A, Ramsay M G, Sircombe N J, Gillies P, Evans R G, Schmitz H, Bell A R and Ridgers C P 2015 *Plasma Phys. Control. Fusion* **57** 113001
[54] Dawson J M, Decyk V K, Huff R W, Jechart I, Katsouieas T, Leboeuf J N, Lembege B, Martinez R M, Ohsawa Y and Ratliff S T 1983 *Phys. Rev. Lett.* **50** 1455
[55] Katsouleas T and Dawson J M 1983 *Phys. Rev. Lett.* **51** 392